Single sensor airborne data sources for forest inventories by tree species

Mikko Kukkonen
School of Forest Sciences
Faculty of Science and Forestry
University of Eastern Finland

Academic Dissertation

To be presented, with the permission of the Faculty of Science and Forestry of the University of Eastern Finland, for public criticism via an online Lifesize conference, on 23rd June 2020, at 16:00 o'clock

2

Title of dissertation: Single sensor airborne data sources for forest inventories by tree species

Author: Mikko Kukkonen

Dissertationes Forestales 297

Thesis supervisors:
Professor Petteri Packalen
School of Forest Sciences, University of Eastern Finland, Finland

Professor Matti Maltamo
School of Forest Sciences, University of Eastern Finland, Finland

Pre-examiners:
Associate Senior Lecturer Eva Lindberg
Department of Forest Resource Management, Swedish University of Agricultural Sciences, Umeå, Sweden

Research Professor Ole Martin Bollandsås
Faculty of Environmental Sciences and Natural Resource Management, Norwegian University of Life Sciences, Ås, Norway

Opponent:
Professor Sorin Popescu
Department of Ecosystem Science and Management, Texas A&M University, College Station, Texas, USA

ABSTRACT

Modern remote sensing-based forest inventory methods utilize airborne light detection and ranging (LiDAR) and optical image data for the prediction of forest attributes by tree species. These methods assume that the three-dimensional information provided by LiDAR can be used to predict the total growing stock attributes, while the spectral reflectance of tree crowns, contained in optical image data, are beneficial for the discrimination of tree species. In Finland, airborne image data has been found suitable for the discrimination of the most common tree species: pine (*Pinus sylvestris*), spruce (*Picea abies*) and broadleaves (mainly *Betula pendula* and *Betula pubescens*). There are, however, numerous issues in the collection and use of two different types of datasets in the inventory process, such as incorrect co-registration of datasets and increased data acquisition and processing costs.

In the wake of advances in algorithms and hardware, two new data sources have been merged as single sensor solutions for tree species-specific forest inventories: stereo matching of aerial images and multispectral airborne LiDAR. Both data sources offer structural and optical information beneficial in tree species classification. However, due to differences in observational geometry, the interpretation, and, thus, the usefulness of the optical information may differ between these two data sources. It is, therefore, essential to examine whether the differences in data characteristics between stereo matching of aerial images and multispectral airborne LiDAR affect the performance of the inventory.

In this thesis, stereo matching data and multispectral airborne LiDAR data are evaluated as single sensor solutions for tree species-specific forest inventories. The results provide a unique insight as to how these data sources compare to the traditional use of single wavelength airborne LiDAR and aerial images. The findings can be used to support future species-specific forest inventories on the selection of remotely sensed data.

Keywords: aerial image, area-based method, multispectral airborne laser scanning, stereo matching

ACKNOWLEDGEMENTS

Joensuu, 2020

Mikko Kukkonen

LIST OF ORIGINAL ARTICLES

This PhD thesis consists of an introductory review followed by three research articles, which are referred to in the summary by their Roman numerals. These papers are reproduced with the permission of the publishers.

I.   Kukkonen M., Maltamo M., Packalen P. (2017). Image matching as a data source for forest inventory – Comparison of Semi-Global Matching and Next-Generation Automatic Terrain Extraction algorithms in a typical managed boreal forest environment. International Journal of Applied Earth Observation and Geoinformation 60: 11–21. https://doi.org/10.1016/j.jag.2017.03.012

II.   Kukkonen M., Maltamo M., Korhonen L., Packalen P. (2019). Multispectral airborne LiDAR data in the prediction of boreal tree species composition. IEEE Transactions on Geoscience and Remote Sensing. 57(6): 3462–3471. https://doi.org/10.1109/TGRS.2018.2885057

III.   Kukkonen M., Maltamo M., Korhonen L., Packalen P. (2019). Comparison of multispectral airborne laser scanning and stereo matching of aerial images as a single sensor solution to forest inventories by tree species. Remote Sensing of Environment. 231: 111208. https://doi.org/10.1016/j.rse.2019.05.027

Mikko Kukkonen was the primary author of all three articles. The primary author conducted most of the data analyses, data preparations and implemented the required modelling routines. Writing of the manuscripts was carried out in collaboration with the co-authors.

TABLE OF CONTENTS

ABBREVIATIONS

ABA	Area-based approach
ALS	Airborne laser scanning
DTM	Digital terrain model
IPC	Image point cloud
ITD	Individual tree detection
LiDAR	Light detection and ranging
M-ALS	Multispectral airborne laser scanning
MD	Mean difference
NGATE	Next-generation automatic terrain extraction
NN	Nearest neighbor
OIF	Optical image feature
RMSE	Root mean square error
SGM	Semi-global matching
U-ALS	Unispectral airborne laser scanning

1 INTRODUCTION

1.1 History of airborne remote sensing in forest inventories

The predominant purpose of forest inventories has been to support forest management and forest resource management with reliable, timely and scalable information of forest resources. This information includes, but is not limited to, basal area, height, volume and tree species. Continuous changes due to natural disturbances and growth (Oliver and Larson 1996), the inherent complexity and the scale of the forests, and the information needs of stakeholders dictate how forest inventories are planned and conducted. Since the early 20th century, auxiliary data sources, such as aerial images, have been used to complement field work and to diversify the information content of the inventory (Andrews 1933; Standish 1945). The first applications of panchromatic aerial images were used as support for transportation planning, in the delineation of forest stands, for the identification of tree species and the measurement of tree heights from oblique and vertical aerial images (Seeley 1934). To this day, aerial images are utilized for most of these tasks, albeit using modern technologies.

In order to further enhance the information content and the value of remote sensing-based forest inventories, characterization of forest structure using airborne laser scanning (ALS) has been practiced since the beginning of the 21st century (Næsset 2002). The adoption of ALS brought about a paradigm shift in the forest inventory community, both in research and operational forestry, which led to increased efficiency, accuracy and cost savings.

1.2 Introduction of LiDAR to forest inventories

Using light amplification by stimulated emission of radiation (LASER), a highly directional and powerful optical light beam can be generated (Young 1986). Distance to an object from the laser source can be determined using the pulse ranging principle (Wehr and Lohr 1999). Because the speed of light is known, this simply entails calculating the travel time of a laser pulse between the emitted and received pulse (Jelalian 1992). By emitting pulses in rapid succession, detailed 3D point observations, referred to as point clouds, of a target structure can be acquired. The realization of range information via laser is widely known as light detection and ranging (LiDAR) and is commonly used as an acronym for all laser ranging systems. Contemporary LiDAR systems usually record multiple echoes per emitted pulse, given that a pulse encounters objects that light can partly penetrate, and the amplitude of the backscatter is sufficiently strong to be registered as an echo.

Rempel and Parker (1964) proposed that LiDAR be used in micro-relief experiments to obtain ground and tree heights. However, it was only in the late 1970s that ground measured tree heights were compared to LiDAR profiles (Solodukhin et al. 1976; Solodukhin et al. 1979). Shortly after, similar experiments were carried out elsewhere (Krabill 1984; Maclean and Krabill 1986). The LiDAR sensors used in these pioneering studies were, by todays standard, very crude (Toth 2009). The sensors had no scanning mechanism, which limited the systems to profiling applications. As LiDAR systems with higher pulse repetition frequencies became available, a scanning laser system could be built where pulses could be directed in a pattern by an oscillating mirror (Wehr and Lohr 1999). This, together with the

introduction of global positioning system (GPS), inertial measurement units (IMU), faster computer processing capacity and better storage solutions, allowed for the collection of 3D georeferenced point cloud data (Nelson 2013). The collection of airborne LiDAR via a scanning sensor would later be known as airborne laser scanning (ALS).

A practical approach to use ALS for the prediction of tree attributes for forest inventories was first developed in Norway (Næsset 1997), shortly after the first commercial ALS systems became available. Statistical characteristics of LiDAR echoes in an area were regressed against field measured stand volume. The method would later be refined (Næsset 2002; Næsset 2004; Maltamo et al. 2006) and become known as the area-based approach (ABA). The ABA follows the assumption that ALS data for a given forest area can be statistically related to its forest attributes. Hence, forest attributes in ABA are predicted by forming a model between the features of ALS point clouds and forest attributes measured from a field plot. The model can then be applied to prediction units, approximately the size of field plots, within the boundaries of the ALS data. Commonly used features describe the vertical distribution of echo heights, such as mean, median, percentiles or densities (e.g. Næsset 2002). Features related to the form of the echo height distribution, such as skewness and kurtosis, have also been used in the prediction of forest inventory attributes (e.g. Levick et al. 2016). As these variables generally describe the vertical structure of the vegetation, the orthometric heights of all LiDAR echoes need to be related to ground level, i.e. subtract the height of the ground from the height of the LiDAR echo. As in this thesis, this is often referred to as height normalization, which can be carried out by identifying ground echoes (see e.g. Axelsson 2000) and constructing a digital terrain model (DTM) from those echoes. Height above ground level (AGL) can then be calculated for all points by subtracting the DTM from the orthometric point height.

Shortly after the inception of ABA, a method was developed where physical properties were modeled for single trees segmented from the 3D data (e.g. Hyyppä and Inkinen 1999; Hyyppä et al. 2001; Persson et al. 2002). The method would later be called individual tree detection (ITD). The basic premise of ITD is to first detect and delineate individual trees from the point cloud data and then predict the attributes of the detected trees. Properties of the segmented trees are determined either directly from the point cloud or by modeling. While it does not necessarily perform better than ABA (Yu et al. 2010), ITD does allow for the prediction of inventory data at a much finer spatial resolution. Nevertheless, because the focus of this thesis is on the applications of new single-sensor airborne data for ABA, ITD is not discussed further here.

1.3 Combining LiDAR and optical data in forest inventories by tree species

Tree species information is required by most forest management systems, due to species-specific growth models and treatment schedules, or management operations that are defined by tree species. It was evident since the early adoption of ABA that tree species could not be predicted using ALS data only (Törmä 2000). This can be attributed to the fact that a field plot, albeit a small area, can consist of several different tree species. Therefore, the structure of the ALS data, or, more specifically the features calculated from the point cloud, do not necessarily explain the tree species distribution.

There have been attempts to predict tree species using ALS data only with ABA. For example, Villikka et al. (2012) reported decreased error rates for conifer and broadleaved stem volumes when using leaf-off ALS data instead of leaf-on ALS data. The rationale was

that the phenology of the deciduous tree species could be exploited to decrease the prediction errors associated with the deciduous trees. The height distributions of LiDAR echoes differ much more in between coniferous and deciduous dominated plots in leaf-off data than in leaf-on data. This results in better tree species discrimination when using LiDAR data only. However, the acquisition period of leaf-off LiDAR data is very narrow between two seasons: spring and summer. Early data collection is affected by snow cover on both the ground and trees. Late data collection, on the other hand, might be affected by emerging leaves on the branches of deciduous trees.

Moreover, LiDAR intensity, i.e. the amplitude of the received pulse (Wehr and Lohr 1999), has been presumed to provide information relevant for target classification as it is an indicator of target characteristics (extent, orientation, density, surface roughness, brightness and reflectance etc.). Because the crowns of different tree species are characterized by distinctive features, such as density, size and orientation of foliage, LiDAR intensity could be beneficial in tree species classification (Ørka et al. 2007). Applications of LiDAR intensity in tree species classification have been mainly studied using ITD (e.g. Korpela et al. 2010b, Cao et al. 2016). LiDAR intensity is affected by a multitude of environmental factors, in addition to target geometry, such as range, sensor configuration, incidence angle and atmospheric conditions (Coren and Sterzai 2006). In part because these factors are not straightforward to correct or to normalize, practical applications of LiDAR intensity in tree species classification, using ABA, have been limited. Moreover, it is not obvious how a complex and mixed tree species composition translates to intensity within an area. Yet, there are a few studies where LiDAR intensity have been used to predict tree species with ABA. For example, Donoghue et al. (2007) showed that intensity could be used to predict the proportion of a specific spruce species.

As means to provide more reliable tree species-specific attributes for forest inventories, optical information of images from both air- and spaceborne platforms have been used together with ALS data. The methods that produce tree species-specific attributes by means of ALS and aerial images using ABA have been developed in Finland (Packalén and Maltamo 2006, 2007, 2008, Kukkonen et al. 2018). The predictions of tree species-specific attributes are usually based on a nearest neighbor imputation (k-nn), where most similar observations, with respect to ALS and image features, are searched from a training sample of field plots. Here, structural information of ALS is assumed to correlate with the total attributes, while the reflectance of tree canopies captured by an image sensor is assumed to contain information relevant for tree species discrimination. The imputation of tree species composition with ABA has been criticized to favor dominant tree species at the expense of minority tree species (Ørka et al. 2013). However, the most notable benefit of the approach is that the attributes of all tree species can be predicted simultaneously, thereby producing predictions of the tree species-specific attributes that are coherent with total growing stock attributes.

Multi-temporal satellite image data can be used in tree species analysis due to phenological differences between tree species (see e.g. Wolter et al. 1995, Hill et al. 2005, Persson et al. 2018). Modern moderate spatial resolution satellite constellations, such as Sentinel-2 and Landsat-8, have high temporal resolutions. Frequent revisits improve the likelihood of capturing unobscured images during phenological activities, which are often swift and dependent on local climate conditions. Although satellite images have considerable potential in tree species analyses, the objective of this thesis is to compare airborne platforms and thus extensive discussion on applications of satellite data for tree species-specific forest inventories is omitted.

To clarify the terminology used in this thesis, the term "optical" is used when referring to passive remote sensing information of aerial images (near infrared, in addition to visible spectrum), and the term "spectral" is reserved for multiple- and single wavelength LiDAR. The term "optical image feature" (OIF) refers to features calculated directly from the aerial images, rather than features calculated from the stereo matching point cloud data.

1.4 Single sensor solutions for forest inventories by tree species

The solution to the tree species problem described in the previous section requires the collection and co-registration of two different types of remote sensing data: LiDAR and aerial images. This can have adverse effects on both the planning and execution of the flight missions and on the properties of the data. Numerous environmental conditions, including solar angle, cloud cover, temperature, precipitation and wind speed, need to be considered when planning optical data acquisition (Pepe et al. 2018). LiDAR data collection, on the other hand, is not as restricted by environmental conditions and can even be acquired during the night when wind speeds are most stable (Gatziolis et al. 2008). Although it is possible to mount both LiDAR and camera sensors on board a fixed wing plane (May 2008; Teledyne Optech 2019), they often have different acquisition parameters with regard to flying altitude, illumination dependence and coverage. Hence, the most sensible solution, in many cases, is to acquire LiDAR data and aerial images separately. Not only is this expensive but can also introduce problems when combining the two data if they have been captured when temporally distant to each other.

Merging data from an active sensor, such as a laser scanner, with a passive sensor, such as a camera, is never straightforward (Wang et al. 2007; Holmgren et al. 2008; Liu et al. 2015; Dash et al. 2017). Airborne LiDAR data and aerial images have been combined in several ways. The most obvious approach is to simply assign Digital Number (DN) values of pixels to corresponding LiDAR points using x and y coordinates (Dash et al. 2017). Assuming that the data has been georeferenced (i.e. orthorectified), the method requires no information about the interior or exterior orientation of images and is, therefore, easy and computationally inexpensive to implement. However, DN values cannot be reliably assigned for elevated targets using this approach due to relief displacement. Also, the original DN values could be altered at multiple stages of orthorectification (Valbuena et al. 2011). Another method is to use collinearity equations (Holmgren et al. 2008; Packalén et al. 2009), where 3D LiDAR points are assigned to a 2D image plane using interior (sensor and optics) and exterior (yaw, pitch and roll) orientation. The method is more reliable for elevated targets but exhibits errors in LiDAR points that are occluded in the image frame and is computationally more expensive than fetching a DN value from an orthorectified image. The errors caused by occluded points can, to a certain extent, be mitigated by averaging the retrieved DN values

Because of the issues outlined above, a single sensor where 3D data and spectral data are recorded simultaneously appears appealing. Recently, two data collection methods have been proposed to provide both structural and spectral information as a single sensor unit: multispectral airborne LiDAR and photogrammetric processing of aerial images to point clouds.

1.4.1 Beyond two dimensional images

The ability to make observations in three dimensions from planar images is not a recent discovery; analog photogrammetry has been practiced for decades (Konecny 1985). However, in the 21st century, the processes of stereo photogrammetry have evolved from analog workstations to a fully digital environment where 3D point clouds, like LiDAR, can be derived from overlapping images. This data will be referred to as image point clouds (IPC) hereafter. In the literature, processes that create depth from stereo images are referred to as, for example, image matching (Haala 2011), stereo matching (Hirschmüller 2008) or digital photogrammetry (St-Onge et al. 2008). In this thesis, the term stereo matching will be used.

Stereo matching is the process of creating depth from overlapping stereo images (Bolles et al. 1987). In this context, depth simply means the distance of an object from the projection center of the camera. The principle of how depth is calculated is similar to the way that depth perception works: when the observer is in motion, the apparent movement of an object at a distance from an observer is less than an object near to an observer. What this means is that when two images are taken of a scene, an object appearing in the right image is at a different location to the same object in the left image. However, this distance is not only a function of the baseline (distance between the cameras), but also of how far away the object is from the camera. Closer objects move a longer distance between the left and right image. For rectified images, this distance is known as disparity (horizontal distance measured in pixels) in computer vision terminology (Okutomi and Kanade 1993). With known disparity, focal length and baseline, a distance from the camera can be calculated. Stereo matching algorithms can be roughly classified into two categories: local methods and global methods. Recently, a new category of deep stereo matching has been established, as convolutional neural networks have been utilized to produce depth images (see e.g. Mayer et al. 2016; Seki and Pollefeys 2017). The basic outline of local stereo matching algorithms is presented in the next paragraph, as the stereo matching algorithms used in this thesis operate using either local methods, or semi-global methods.

A disparity calculation requires the observation of the same target from two images. This is a trivial task for a human operator but can be incredibly difficult for an algorithm. There are several algorithms with different implementations that have been developed for this purpose (e.g. Hirschmüller 2008; Jin and Maruyama 2012; Chen and Li 2017). In general, local stereo matching algorithms are applied to rectified image pairs and they have four distinct steps: (1) initial cost calculation, (2) cost aggregation, (3) disparity computation and (4) disparity refinement. Here, cost means the similarity of a pixel in the left and right image. The lower the cost, the more similar the pixels. Usually pixel-wise cost calculation is far too noisy. Hence, some other indices are used, such as mutual information (Hirschmüller 2008), or area-based matching of a rectangle surrounding the pixel using, for example, correlation (Gupta and Cho 2010) or hamming distance of census transformed pixels (Lim et al. 2016). In step (1), a cost is calculated for every pixel (x_1, y_1) in the base image with respect to every pixel in row y_1 in the matched image. In step (2) the costs are smoothed using a chosen aggregation function (Tombari et al. 2008), and afterwards the disparity is calculated for each pixel in step (3) using a chosen strategy (e.g. winner takes all), thus resulting in an initial disparity image/map. In step (4), the noise and outliers in the disparity image are removed, for example, by a median filter or a left to right consistency check. The steps described in this paragraph are approximate designs, and different implementations have different strategies, therefore the stereo matching algorithm chosen for this thesis will be explained later in more detail in Section 2.3.1.

Stereo matching offers both structural and optical information as a single instrument. It has the benefit of providing optical information from the same geometry as the point cloud and does not have the shortcomings of combining ALS and image data, as explained in Section 1.2. However, the exact method of how the DN values of images are assigned to IPC data is proprietary in most commercial software, thus limiting its suitability in scientific analyses. Also, as images can only view the surface of an object, IPC data does not portray structure like LiDAR (White et al. 2013). LiDAR penetrates the canopy, often recording multiple echoes per emitted pulse, thus providing a rather even representation of the vertical structure and the ground (Lefsky et al. 2002). On the other hand, IPC data provides a detailed description of the above visible canopy and, when visible, the ground. Observing the ground underneath the canopy layer can be quite difficult in dense forests, requiring an alternative method for height normalization, such as ALS data.

1.4.2   Stereo matching in forest inventories

Although prediction errors associated with total growing stock volumes have generally been greater using IPC data, when compared to ALS data (e.g. Bohlin et al. 2012; Järnstedt et al. 2012; Straub et al. 2013; Vastaranta et al. 2013; Yu et al. 2015), this might not have adverse effects on the timing of forest management operations (Kangas et al. 2018). The reason that total growing stock volume is predicted with larger errors using IPC compared to ALS could be, for example, the result of how inconsistent illumination affects the generation of IPC data (St-Onge et al. 2008; Gobakken et al. 2015). However, White et al. (2015) have concluded that no systematic difference in regard to the outcome of ABA was observed in their study area between IPC data acquired from different dates with different solar angles. The reason for the discrepancy in prediction errors associated with total volume can also be attributed to topography, data acquisition parameters or photogrammetric processing strategies, as some studies have reported rather similar prediction errors using IPC data and ALS data (Pitt et al. 2014; Puliti et al. 2017; Ullah et al. 2017; Giannetti et al. 2018).

While the total growing stock volume is not necessarily as highly relatable to features calculated from IPC data than from ALS data, the use of both structural and optical features can be beneficial in the prediction of tree species-specific attributes, as already discussed in Section 1.3. Tuominen et al. (2017) reported prediction errors (RMSE) of 59.8–142.2 % for tree species volumes using IPC and optical image features, and 57.3–136.0 % using IPC and satellite image features at the plot-level in a study site in central Finland. Puliti et al. (2017) reported plot-level prediction errors of 48.9–113.8 % for tree species-specific volumes from a forest located in south-eastern Norway using IPC and OIF.

Even though stereo matching data are usually notably cheaper than ALS data, the use of IPC as a data source in forest inventories often assumes that ALS data is available for the inventory area, as DTM derived from IPC data can be prone to errors in areas of dense canopy. The search for ground points can incorrectly assign canopy points as ground in places where the ground surface is occluded over large areas. Also, interpolation within the DTM can be inaccurate if extensive areas of ground surface are hidden beneath the canopy. There have been experiments where IPC-derived DTM was used to normalize point heights to the ground level (Alonzo et al. 2018). Also, the use of DTM-independent features for the prediction of total growing stock volumes using IPC has been explored recently (Giannetti et al. 2018). However, neither approach conclusively answers whether they can be applied in areas where a significant proportion of the forests have a closed canopy. Nonetheless, open-access nationwide ALS data is currently readily available in many countries. As topography

rarely changes drastically over time, even quite dated ALS-based DTM is suitable for the height normalization of ALS echoes.

1.4.3 LiDAR in multiple wavelengths

The first commercial airborne multispectral ALS sensor, Optech Titan (Teledyne Optech 2019), captures LiDAR data in three different wavelengths: 1550 nm (channel 1), 1064 nm (channel 2) and 532 nm (channel 3). Commercial dual-wavelength airborne LiDAR systems have been available, although their primary applications have been to capture geospatial data of the coastline and shallow waters. Multispectral airborne LiDAR will be referred to as M-ALS (multispectral airborne laser scanning) hereafter. Not only does M-ALS increase the echo density of the point cloud but, in theory, also allow for more accurate tree species discrimination compared to traditional single wavelength (hereafter unispectral) ALS systems (see Section 1.1). This means, for example, that the ratios of different LiDAR channels could be beneficial in classification. It should be noted, however, that intensity is also affected by other factors in addition to reflectance characteristics, such as observational geometry and target shape (e.g. Korpela et al. 2010a).

The Optech Titan is comprised of three laser transmitters. The laser transmitters are slightly angled with respect to each other: the 1064 nm channel is pointing nadir, the 1550 nm channel 3.5 degrees forward and the 532 nm channel 7.0 degrees forward. This means that it does not observe the exact same target location at all wavelengths. As a result, the spectral information provided by the Optech Titan cannot be interpreted with the same rationale as a conventional passive sensor. Point-wise analyses are thus unrealistic because the exact same target area is very rarely observed from all three channels. Hence, methods that classify objects, such as individual trees (ITD) or field plots (ABA) should be more appropriate.

1.4.4 Multispectral LiDAR in forest inventories

At the time of preparing this thesis, M-ALS is not yet operational in forest inventories. The adoption of the technology is not only limited by a lack of research, but also by the fact that the collection of the M-ALS data is currently more expensive than the collection of both unispectral LiDAR and aerial images. Increased costs can, in addition to more valuable hardware, be attributed to the fact that M-ALS data need to be acquired at a lower acquisition altitude than the traditional 1064 nm or 1550 nm single wavelength LiDAR data. Lower flying altitudes are required in order to obtain comprehensive data from the 532 nm channel.

Initial research on forest inventory applications of M-ALS were aimed at confirming the assumption that M-ALS intensity would be analogous to optical information of aerial images by classifying individual tree species. In their study, Yu et al. (2017) classified pine, spruce and broadleaved trees and reported overall accuracy (OA) of 85.9 % for 1167 detected (detection rate 61.3 %) trees using both structural and intensity features of M-ALS. Axelsson et al. (2018) classified 179 mature solitary trees from nine genera and obtained 76.5 % OA using both intensity and structural features of M-ALS data. Budei et al. (2018) found that the combined features from all three channels provided the highest classification accuracy (75 %) in the classification of 10 manually delineated tree species. The only experiments to date where M-ALS data has been applied using ABA were published by Dalponte et al. (2018) and Räty et al. (2019). Dalponte et al. (2018) found that M-ALS data provided better results than conventional ALS data in predicting a variety of forest characteristics, including the

Shannon diversity index (SDI) of tree species. The SDI was predicted with the lowest error rate by calculating the predictor variables, considering all echoes across all channels. In contrast, Räty et al. (2019) reported that a combination of LiDAR and aerial images were superior to M-ALS data in the prediction of tree species-specific logwood volumes in Finland.

In all previous studies, M-ALS provided better results when compared to unispectral ALS. All current research is in agreement that intensity information from the three channels is advantageous in tree species classification. However, based on the current literature, it is not yet obvious how, or to what extent, M-ALS data would benefit forest inventories by tree species using ABA.

1.5 Objectives of this PhD thesis

The main goal of this PhD thesis is to assess whether single sensor data (stereo matching or M-ALS) are beneficial in forest inventories. In more detail, the objectives are:

i.   Evaluate how IPC data, combined with optical image features, performs in predicting forest inventory attributes, compared to unispectral leaf-on or leaf-off ALS data combined with optical image features (Study **I**).

ii.   Assess how M-ALS data compares to the use of aerial images and unispectral leaf-on or leaf-off LiDAR data in the prediction of boreal tree species composition. (Study **II**).

iii.   Compare IPC and M-ALS data in the prediction of tree species-specific volumes (Study **III**).

2 MATERIALS

2.1 Study areas

Two boreal forest areas were used in this thesis, hereafter referred to as Hamina (study **I**) and Liperi (study **II** & **III**) (Figure 1). Hamina is located in Kymenlaakso, whereas Liperi is located in the region of North Karelia, Eastern Finland. The main tree species in both study areas are Scots pine (*Pinus sylvestris*), Norway spruce (*Picea abies*) and broadleaved tree species, namely downy birch (*Betula pubescens*) and silver birch (*Betula pendula*). Both study areas are predominantly privately owned, with timber production the main objective of forest management and planning.
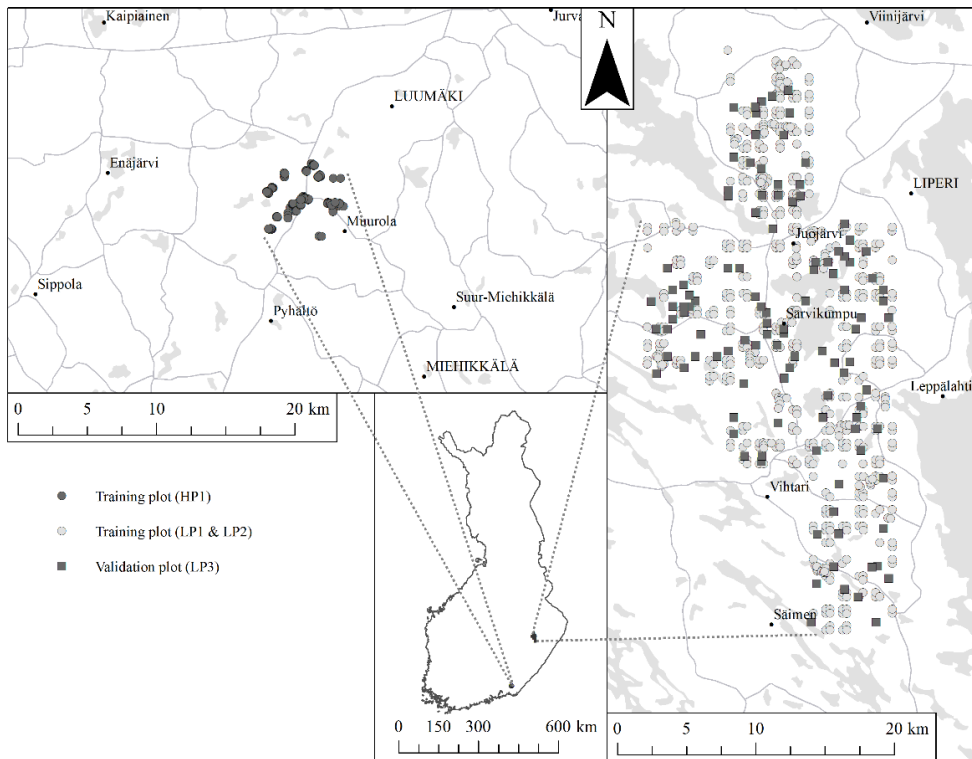
Figure 1. Study areas and field plots.

2.2 Field data

Field data from four different field campaigns are used in this thesis. One field campaign was conducted in Hamina (HP1) and three in Liperi (LP1, LP2, LP3). Field data were collected from Hamina during the summer 2013 (HP1). The radius of the plot was either 9 m or 12.62 m depending on the number of trees observed within the 9 m radius. Diameter was measured for every tree with a diameter at breast height (DBH) of at least 5 cm. Height was measured for a subset of trees. Heights for the remaining trees were calculated using the functions based on Näslund (1937) model form.

Table 1. Field data used in studies **I** – **III**.

Study	Field data
I	HP1
II	LP1, LP2
III	LP1, LP2, LP3

Field data from Liperi were collected during summers 2016 (LP1 & LP2) and 2017 (LP3). In LP1, field plots were selected by systematic sampling, and trees within the field plots were measured using the same general strategy. The LP1 study area consisted of circular field plots in systematically sampled square-shaped clusters of four plots. The distance between the plots was 300 m and the distance between clusters was 1200 m. The radius of the plot was either 9 m or 12.62 m depending on the number of trees observed within the 9 m radius. The radius was increased to 12.62 m if there were < 20 trees within the 9 m radius from the plot center. In LP1, tree species, height and DBH were measured for all trees with a DBH ≥ 5cm. LP3 consisted of 30 m x 30 m square plots that were non-probability sub-sample from an original systematic sample using information in regard to development classes and dominant tree species at the plot-level. Trees were measured with the same strategy as in LP1, with the difference that the location of each tree was determined using the approach described in Korpela et al. (2007). With known locations for each measured tree, the 30 m x 30 m plots were divided into four 15 m x 15 m cells.

The LP2 field plots were measured as part of an operational forest management inventory (FMI) conducted by the Finnish Forest Centre (SMK). The LP2 plots were distributed in L-shaped clusters. The field plots were measured with the same general strategy as in LP1 and LP3, except that heights were measured for a subset of trees, as opposed to all trees. These sample trees were selected by tree species based on the observed diameter distribution at the plot. Locally calibrated multivariate linear mixed-effects model (Eerikäinen, 2009) was used to calculate the heights for the remaining trees. The stem volumes of trees were calculated as a function of diameter and tree height using the models of Laasasenaho (1982).

The different field data used in the studies are presented in Table 1. The LP1 field plots are used in studies **II** and **III**, although, different subsets of field plots were used. The reason for this was due to the differences in prediction methods and response variables. Because the dominant tree species was predicted using a linear classifier in **II**, only field plots located entirely within a single forest stand were used. This decision did not exclude mixed species forest stands, but rather plots that would bring about unwanted effects due to different forest management operations. These field plots were later included in **III**, because *k*-nn was used with separate validation field plots.

2.3 Remotely sensed data

2.3.1 Airborne laser scanner data and aerial images

A total of three different ALS datasets and two aerial image datasets were used in this thesis. The acquisition parameters of the ALS data are presented in Table 2 and the acquisition parameters of aerial images are presented in Table 3. The true point density of the Optech Titan data used in this thesis is greater than stated in Table 3, as the lateral overlap of adjacent flight lines of the data was over 50 %. In all ALS data, echoes were classified as ground and non-ground echoes with the method described in Axelsson (2000), and afterwards, the ground echoes were used to construct a DTM. The AGL heights for all echoes were then calculated by subtracting the DTM from orthometric echo heights.

The intensity values of all three bands of Optech Titan were corrected for range. Details of the range correction are presented in study **II**. Range corrected intensity values were used in studies **II** and **III**.

Table 2. Summary of airborne laser scanning (ALS) acquisitions. PRF = pulse repetition frequency, mrad = milliradian.

	Optech Titan			Leica ALS60	Leica ALS70
	1550nm	1064nm	532nm		
Acquisition date	2–10 July 2016	2–10 July 2016	2–10 July 2016	3 May 2016	25 June 2013
Studies	II & III	II & III	II & III	III	I
Flying altitude (m)	~850	~850	~850	2400	1900
Scan angle (degrees)	±20	±20	±20	±20	±20
PRF (kHz)	250	250	250	98.4	67.6
Beam divergence (mrad, 1/e)	0.35	0.35	0.70	0.15	0.15
Pulse density (per m^2)	4.8	4.8	3.7	0.8	0.75

Table 3. Summary of aerial image acquisitions. Hyphen indicates unknown.

	DMC Z/I Intergraph		Microsoft Ultracam XP
	Multispectral	Panchromatic	
Acquisition date	23–24 May 2016	23–24 May 2016	12 June 2013
Studies	II & III	III	I
Flying altitude (m)	4100	4100	6000
Sensor size (pixels)	3456 × 1920	13824 x 7680	17310 x 11310
Focal length (mm)	30	120	100
Spectral bands	Red, green, blue and NIR	Pan	Red, green, blue and NIR
GSD (cm)	150	40	35
Side-/endlap (%)	30 / 80	30 / 80	45 / 80

2.3.2 Stereo matching of aerial images

In this thesis, stereo matching of aerial images was carried out using two different matching algorithms: The Semi-Global Matching (SGM) algorithm (Hirschmüller 2008) and Next-Generation Terrain Extraction (NGATE; Zhang et al. 2007). In study **I**, SGM and NGATE were compared, whereas only SGM was used in study **III**. A general outline of the matching process, i.e. disparity computation, is given Section 1.4.1.

SGM has been widely recognized as a robust stereo matching algorithm that produces matching accuracies comparable to global matching methods at a much lower computational complexity (Hirschmüller 2008; Hirschmüller et al. 2012). The novel idea of SGM lies in the optimization, or aggregation, of pixel disparities after the initial disparity calculation (discussed in Section 1.3.1). SGM proposes that the NP-hard optimization problem of global stereo matching could be estimated by two-dimensional scanline optimization. Instead of traversing a single line, SGM performs the optimization in multiple directions at each pixel. Penalties for both small and large disparity differences along the lines between neighboring pixels are enforced in the optimization. If the disparity difference between the previous pixel and the current pixel in a scan line is > 1, a larger penalty is added to the cost of the disparity at the current pixel. After all scanlines have been calculated, the smallest aggregated cost is chosen for each pixel.

NGATE is among the most common stereo matching algorithms reported in literature. Unfortunately, the way that NGATE performs the matching is not described in detail, because it is a proprietary algorithm of BAE Systems. It was reported in Zhang et al. (2006 & 2007) that NGATE combines two algorithms in the matching process: area-based image correlation and edge matching. Image correlation is used to constrain and guide the edge matching and vice versa. It is not known, however, how these two algorithms operate or complement each other in greater detail.

Different parameter combinations were tested with both NGATE and SGM. In SGM, the only configurable parameter was the color band that was to be used in the matching. In NGATE, different combinations of parameters were tested. These parameters included the window size, algorithm (image correlation and/or edge matching) and the use of adaptive correlation strategy. Only the results of the most optimal parameter combinations, with respect to prediction error, are reported here.

3 METHODS

3.1 Feature extraction

Features used in the modeling can be divided into point cloud features and OIF. All point cloud features, both LiDAR and stereo matching, were calculated from AGL point cloud data, and OIF were computed by first linking points to unrectified images. In study **I**, stereo matching features were calculated separately using a low-resolution (10 m resolution pre-ALS era, hereafter "10m DTM") and high-resolution "ALS DTM" in order to assess the feasibility of applying stereo matching data in geographical areas where LiDAR data is unavailable.

3.1.1 Point cloud features

Point cloud features were calculated from both ALS and IPC data using the same procedure. While not explicitly stated in Table 4, point cloud features were calculated separately for first-of-many + only (F), and last-of-many + only (L) echo classes in the case of LiDAR data. From the stereo matching data, point cloud features were calculated using all point observations. IPC data do not contain intensity features. M-ALS features include ratios of point cloud features from different channels and point cloud features calculated from a combined set of echoes from different channels.

Table 4. Features of LiDAR and aerial images. Multispectral LiDAR (M-ALS) point cloud features were computed separately for each channel, for each combination of 2–3 channels and ratios of channels. Abbreviations: h = height; i = intensity; ai = aerial image; R = red; G = green; B = blue; N = near infra-red; DN = digital number. Channel number is depicted in the subscript in the case of M-ALS features.

Feature	Description
I – Cloud features from LiDAR and IPC	
hP10, hP20, … , hP90	Height percentiles
iP10, iP20, … , iP90	Intensity percentiles
hD1, hD2, hD5, hD10, hD15, hD20	Density at a fixed height
iMax, hMax	Maximum
iMin, hMin	Minimum
iStd, hStd	Standard deviation
iMed, hMed	Median
iMean, hMean	Mean
iSkew, hSkew	Skewness
iKurt, hKurt	Kurtosis
Prop	Echo class proportion
II – M-ALS features	
I_{532}; I_{1064}; I_{1550}	Single channel features (I)
I_{1550} / I_{1064}; I_{1550} / I_{532}; I_{1064} / I_{532}	Ratios of single channel (I) features
$I_{1550+1064}$; $I_{1550+532}$; $I_{1064+532}$; $I_{1550+1064+532}$	Single channel features (I) computed from combined set of echoes from different channels
III – Optical image features	
aiMax $_{B;G;R;N}$	Maximum DN
aiMin $_{B;G;R;N}$	Minimum DN
aiStd $_{B;G;R;N}$	Standard deviation of DNs
aiMean $_{B;G;R;N}$	Mean DN
aiMax$_{B/G}$, aiMax $_{B/R}$, …, aiMean $_{R/N}$	Ratios of spectral image features

3.1.2 Optical image features

Collinearity equations were used to attach optical information from unrectified aerial images to 3D points using a similar method as described in Packalén et al. (2009). The same method was used with both the IPC and LiDAR data. The channel-wise (red, green, blue and near-infrared) DN value from different images for each LiDAR echo was averaged from all images in which the 3D point was observed. These values were then used to calculate the OIF (Table 4).

3.2 Prediction methods

3.2.1 Linear regression

A linear regression model fit by ordinary least squares was used in study **I** to predict stem number, basal area, DGM, HGM and total volume at the plot-level. For each response variable and each data source, the number of predictor variables was fixed to three. This was carried out to avoid overfitting and to exclude the effect that differences in the number of predictor variables have on model performance.

3.2.2 LDA classification

In study **II**, dominant tree species with respect to stem volume was determined at the plot-level for pine, spruce or broadleaved trees. Linear discriminant analysis (LDA) was used as a classifier. LDA is methodologically similar to ANOVA (analysis of variance) and linear regression analysis. While the dependent variable is continuous in ANOVA and linear regression analysis, LDA deals with categorical variables. The objective of LDA is to find a linear combination of features that primarily characterize or separate two or more classes from one another (Hastie et al. 2009). The initial test showed that five features provided a good compromise between model performance and overfitting.

3.2.3 k-nn imputation

In studies **II** and **III**, the proportions of tree species and tree species volumes, respectively, were predicted using *k*-nn imputation. In both studies, the most similar neighbor (MSN) (Moeur and Stage 1995) distance metric was used to determine the *k*-nn from the training data. This method is often referred to as *k*-MSN. It is a nearest neighbor method, where the distance to neighbors is determined with a weighting matrix produced by canonical correlation analysis. The method is explained in more detail in Packalén and Maltamo (2007). In all *k*-nn models, the prediction is calculated as the weighed mean of the nearest neighbors. In study **II**, tree species proportions were imputed simultaneously for all tree species, as is typical in *k*-nn (e.g. Packalén and Maltamo 2007). However, in study **III**, volumes by tree species were imputed separately for all tree species in order to make the predictions comparable between data combinations. The prediction for total volume was calculated as the sum of the species-specific volume predictions.

3.3 Variable selection

Different variable selection strategies, dictated by the complexity of the optimization task, were used with the prediction methods. Two different approaches for variable selection were applied: a combination of stepwise and exhaustive variable selection, and heuristic variable selection. In all studies, the usefulness of OIF as predictor variables was evaluated by performing variable selection and performance assessment separately for only point cloud features and for point cloud features complemented with OIF.

3.3.1 Linear regression

It would be ideal that all combinations of predictor variables could be assessed when choosing predictor variables for a model. However, it is often impossible to deterministically select an optimal subset of predictor variables from a large population, as the number of potential combinations of variables quickly increase to a point where it is impractical to test them all. In study **I**, predictor variables for the linear regression models were selected by first decreasing the number of potential variables to a maximum of 50 using the stepwise feature selection. After this, all possible combinations of three variables were assessed with RMSE as criterion. Different transformations for the predictor variables and response were calculated prior to variable selection: square root, exponential (only predictor variables) and natural logarithm.

3.3.2 LDA and k-nn

Features for LDA and k-nn models were selected using heuristic optimization. A simulated annealing algorithm, similar to the algorithm in Packalén et al. (2012), was implemented. A crucial aspect in variable selection using a heuristic algorithm is how the current solution should be modified. The algorithm gradually decreases the number of variables replaced from the current solution as a function of temperature. In the beginning, 50 % of the variables were randomly replaced. Thereafter, the number of variables to be randomly replaced was obtained by multiplying the current number of variables to be replaced by the temperature (values ranging from 0.05–1.0). A minimum of one variable was replaced at any given time. This means that as the algorithm converges, fewer variables are replaced by others. Also, the probability to accept a worse solution, often referred to as acceptance probability, decreases as a function of temperature. When the lowest allowed temperature has been reached, in this case 0.05, the algorithm terminates.

3.4 Performance assessment

The various data sources and data combinations evaluated in this thesis are listed in Table 5. All point cloud data were evaluated with and without OIF. The OIF were calculated using the same procedure in all studies. In studies **I** & **II**, prediction performances were validated using plot-level leave-one-out cross validation (LOOCV). In study **III**, k-nn models were validated using independent validation plot data (LP3). Forest attributes were first predicted for the smaller 15 m x 15 m rectangular prediction units. Predictions for the 30 m x 30 m plots were aggregated from the four prediction units within them. A similar aggregation, albeit with a larger set of prediction units, is used in practical applications where predictions of forest attributes are calculated from cells for forest compartments using ABA.

Table 5. Point cloud data sources used in this thesis.

Abbreviation	Definition	Study
Leaf-off-U-ALS	Unispectral leaf-off airborne LiDAR	**II & III**
Leaf-off-U-ALS$_{(+OIF)}$	Unispectral leaf-off airborne LiDAR and optical image features	**II & III**
Leaf-on-U-ALS	Unispectral leaf-on airborne LiDAR	**I - III**
Leaf-on-U-ALS$_{(+OIF)}$	Unispectral leaf-on airborne LiDAR and optical image features	**I - III**
M-ALS	Multispectral airborne LiDAR	**II & III**
M-ALS$_{(+OIF)}$	Multispectral airborne LiDAR and optical image features	**II & III**
IPC	Airborne image point cloud	**I & III**
IPC$_{(+OIF)}$	Airborne image point cloud and optical image features	**I & III**

Prediction strategies were similar in all studies; predictions were produced as an average of several variable selections. The intention of this decision was not to construct ensemble models, but rather to lessen the unwanted effects of randomness due to the heuristic nature of simulated annealing, or in the case of linear modeling, account for randomness due to bootstrapping of samples. The number of iterations varied depending on the computational complexity and the number of candidate predictor variables. In study **I**, predictions were calculated as the average result of 1000 iterations of features selection using a random bootstrap sample (n = 172) in each iteration. In study **II**, predictions were computed using the average values of over 1000 iterations of features selection in the classification of dominant tree species and over 100 iterations of features selection in the prediction of tree species proportions. In study **III**, predictions of volume by tree species were averaged over 100 iterations of features selection.

Prediction errors were assessed in all studies with root mean square error (RMSE%) and in study **III** with mean difference (MD) as well. As MD is calculated as the difference between the means of predicted and observed values, it is mathematically equivalent to bias. The classification accuracies of dominant tree species in study **II** were assessed with producer's accuracy (PA), user's accuracy (UA), overall accuracy (OA) and Cohen's Kappa. The current practice in Finland is to utilize a combination of ALS data (single wavelength, leaf-off or leaf-on) and aerial images. This was used as the performance baseline in this thesis

4 RESULTS

4.1 Stereo matching in the prediction of forest inventory attributes (I)

A comparison of the performance of NGATE and SGM based point clouds, and ALS data in the prediction of selected forest attributes is presented in Table 6. As expected, ALS data consistently outperformed the stereo matching data with all response variables both with and without OIF. The inclusion of OIF did not noticeably affect the prediction errors. The differences between ALS and stereo matching data were most apparent in the prediction errors associated with volume (20.4 % vs. 28.6 %), basal area (18.1 % vs. 26.6 %) and stem number (29.6 % vs. 42.6 %).

Table 6. Summary of root mean square error (RMSE%) values of linear regression models of various forest attributes over 1000 bootstrap samples using Next-Generation Terrain Extraction (NGATE), Semi-Global Matching (SGM) algorithms, and airborne laser scanning (ALS) data both with and without optical image features (OIF). The parameter combination of NGATE or the spectral band of SGM that yielded the lowest error rate is presented and is marked inside parenthesis. I–IV indicates the four different parameter combinations of NGATE, N = near-infrared, R = red, G = green.

	Response	NGATE	SGM	Leaf-on-U-ALS
ALS DTM 3D	Stem number	47.9 (I)	46.7 (N)	31.4
	Basal area	27.4 (III)	26.6 (R)	18.1
	DGM	14.2 (II)	15.0 (R)	13.6
	HGM	8.6 (I)	10.0 (R)	5.7
	Volume	28.6 (III)	29.5 (G)	20.5
ALS DTM 3D + OIF	Stem number	42.6 (III)	42.8 (R)	29.6
	Basal area	26.6 (III)	26.6 (R)	18.2
	DGM	14.5 (II)	16.0 (R)	13.6
	HGM	8.9 (II)	10.7 (N)	5.9
	Volume	27.9 (III)	29.3 (G)	20.4
10m DTM 3D	Stem number	54.9 (I)	49.9 (R)	-
	Basal area	27.6 (III)	26.6 (R)	-
	DGM	30.5 (I)	23.0 (G)	-
	HGM	22.6 (III)	16.4 (G)	-
	Volume	29.1 (III)	29.8 (R)	-
10m DTM 3D + OIF	Stem number	44.1 (II)	43.7 (N)	-
	Basal area	27.0 (III)	26.9 (R)	-
	DGM	20.6 (II)	20.1 (R)	-
	HGM	16.1 (III)	15.6 (R)	-
	Volume	29.0 (III)	30.0 (G)	-

The differences in the prediction errors between the two stereo matching algorithms, or even between the various parameter combinations of NGATE and the spectral bands of SGM, were minor and neither consistently outperformed the other (Table 6). However, when using the 10m DTM in the normalization of stereo matching point clouds, SGM yielded the lowest error rates for every response variable except volume. In contrast, NGATE seemed to perform better when ALS DTM and OIF were used. As was the case with ALS data, stereo matching data did not noticeably benefit from OIF when ALS DTM was used. Interestingly, the inclusion of OIF led to a noticeable decrease in the prediction errors associated with stem number, DGM and HGM when using NGATE stereo matching data normalized with low-resolution DTM. The same was true when using SGM, albeit the decrease in prediction error was less, as the prediction errors were already lower compared to NGATE.

Prediction errors associated with basal area, stem number and volume were not noticeably influenced by the resolution of the DTM. Similar prediction errors were observed for these forest attributes using both LiDAR and 10m DTM with NGATE and SGM. In contrast, the use of 10m DTM resulted in a noticeable increase in the prediction error associated with DGM and HGM, compared to the use of ALS DTM.

4.2 Prediction of tree species composition using M-ALS (II)

4.2.1 Classification of dominant tree species

The plot-level leave-one-out cross validated classification results for dominant tree species are presented in Table 7. The benefit of OIF was greater with leaf-on-U-ALS than with M-ALS. The classification accuracies of pine and spruce were high in all four feature groups. Optical image features mainly contributed to the increase in discrimination of the broadleaved class. Likewise, multispectral LiDAR provided considerably better classification results (UA 78.2 %; PA 51.1 %) for the broadleaved class when compared to U-ALS data (UA 74.0 %; PA 16.8 %). The inclusion of OIF always resulted in the greatest classification accuracies. The M-ALS alone performed almost as well as leaf-on-U-ALS$_{(+OIF)}$ (Kappa 0.79 vs. 0.81, respectively).

Table 7. Classification accuracies associated with the different data combinations. OA denotes overall accuracy, UA denotes user's accuracy, PA denotes producer's accuracy and OIF denotes optical image features.

	Kappa	OA	Pine		Spruce		Broadleaved	
			UA	PA	UA	PA	UA	PA
Leaf-on-U-ALS	0.72	85.0	91.5	92.0	79.4	95.7	74.0	16.8
Leaf-on-U-ALS$_{(+OIF)}$	0.81	89.1	93.7	92.2	85.1	94.5	86.0	57.0
M-ALS	0.79	88.2	92.2	91.7	85.7	94.5	78.2	51.1
M-ALS$_{(+OIF)}$	0.81	89.7	93.6	92.6	86.6	94.0	84.6	62.4

4.2.2 Feature importance

Features of the LDA models of dominant tree species were ranked by the frequency in which they were included in the model. A feature was regarded as important if it was chosen frequently over a large number of iterations by the heuristic variable selection. The five most frequently chosen features by dataset are presented in Table 8. Intensity features were ranked high, especially when using M-ALS or M-ALS was complemented with OIF. The kurtosis and skewness of height distribution were also ranked high in all data sources. It is worth noting that the kurtosis of channel 2 intensities from last echoes was top ranked in all datasets and their combinations.

Table 8. Features importance with different datasets and their combinations. Frequency represents the percentage of linear discriminant analysis (LDA) models containing that variable out of the total 1000 iterations. OIF denotes optical image features. Explanations for the abbreviations of features can be found in Table 5.

	Five most frequent features	Frequency (%)
U-ALS	$iP90_{F1064}$	65.0
	$iKurt_{F1064}$	60.5
	$Prop_{F1064}$	56.5
	$iP70_{F1064}$	51.5
	$hSkew_{L1064}$	20.4
U-ALS$_{(+OIF)}$	$iKurt_{F1064}$	56.6
	$aiMean_{N1064}$	53.7
	$iP70_{F1064}$	34.4
	$Prop_{F1064}$	25.8
	$hStd_{L1064}$	25.7
M-ALS	$iKurt_{F1064}$	43.5
	$iP50_{F1550+532}$	38.4
	$iMed_{F1550+532}$	35.4
	$iKurt_{F1064+532}$	31.8
	$hSkew_{L1550+532}$	22.4
M-ALS$_{(+OIF)}$	$iKurt_{F1064}$	51.4
	$aiMean_{N1064}$	25.5
	$hSkew_{L1550+532}$	22.1
	$aiMean_{RG532}$	20.5
	$iP60_{L1550/1064}$	19.8

4.2.3 Proportions of tree species

The proportions of tree species at the plot-level were predicted simultaneously for pine, spruce and broadleaved trees using *k*-nn imputation. The results are presented in Table 9. Both leaf-on-U-ALS$_{(+OIF)}$ and M-ALS$_{(+OIF)}$ provided considerably lower RMSE values for the broadleaved class than the data sources without OIF. The prediction errors associated with the other classes was also reduced with the inclusion of OIF. The M-ALS data yielded lower prediction errors compared to leaf-on-U-ALS, especially in the case of broadleaved trees.

Table 9. Species proportion predictions with nearest neighbor (*k*-nn) imputation with (+OIF) and without (-OIF) optical image features. Root mean square error (RMSE; percentage points, p.p.) values between observed and predicted species proportion are presented.

	Pine		Spruce		Broadleaved	
	-OIF	+OIF	-OIF	+OIF	-OIF	+OIF
Leaf-on-U-ALS	19.0	16.7	20.5	19.3	22.6	15.4
M-ALS	18.2	16.0	19.5	17.8	19.5	15.0

4.3 Prediction of volume by tree species with stereo matching and LiDAR (III)

Prediction errors associated with tree species volumes and total volume using the different ALS and IPC data in the Liperi study area are presented in Figure 2. Prediction errors associated with total volume were rather similar when using the different ALS datasets. The IPC data yielded the highest prediction errors of total volume, both with (26.7 %) and without (28.8 %) OIF. The prediction errors of pine and broadleaved trees decreased noticeably when OIF were used. The prediction errors associated with total volume and spruce volume were only slightly decreased by the addition of OIF in all point cloud datasets.
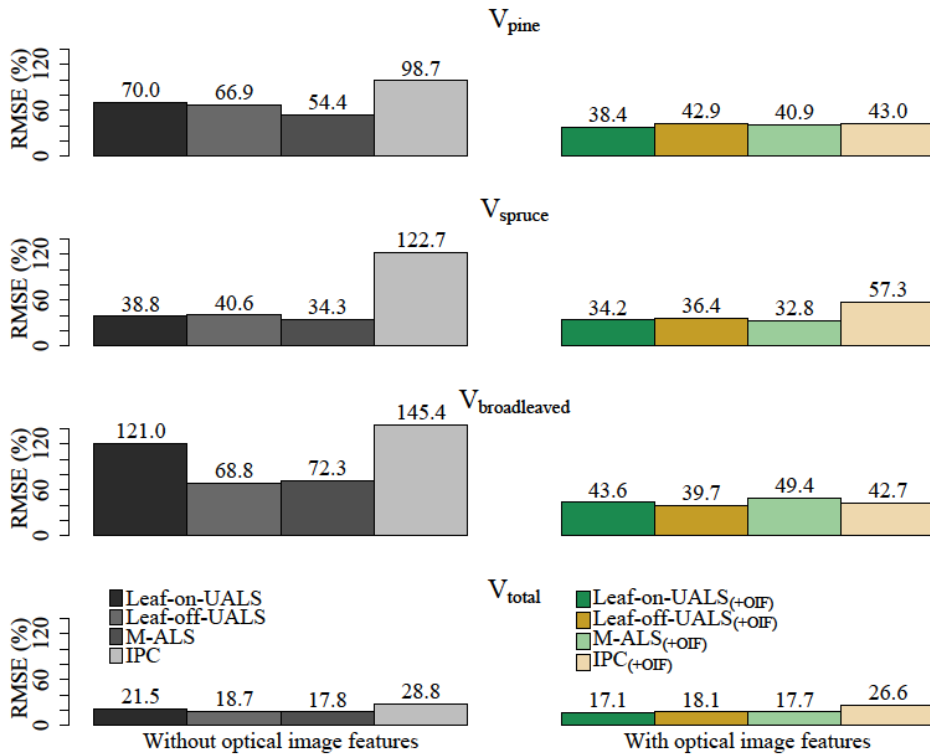
Figure 2. Prediction errors for species-specific volume (V_{pine}, V_{spruce} and $V_{broadleaved}$) and total volume (V_{total}) using leaf-off unispectral airborne laser scanning, leaf-on airborne laser scanning, multispectral airborne laser scanning (M-ALS) and image point clouds (IPC) data with and without optical image features (OIF) in the validation plots.

Prediction errors associated with volumes were, in general, rather similar between the tested single-sensor solutions, IPC$_{(+OIF)}$ and M-ALS. With respect to pine and broadleaved, IPC$_{(+OIF)}$ yielded lower error rates than M-ALS. M-ALS data, however, yielded lower prediction errors for total volume and for spruce volume. When examining the mean of prediction errors across all response variables (Table 10), IPC$_{(+OIF)}$ performed marginally better than M-ALS (42.4 % vs. 44.7 %). However, based on this overall performance, these single-sensor alternatives were clearly poorer compared to leaf-on-U-ALS$_{(+OIF)}$ (33.3 %) and leaf-off-U-ALS$_{(+OIF)}$ (34.3 %).

Prediction errors were lower with M-ALS (mean RMSE: 44.7 %) than leaf-off-UALS (mean RMSE: 48.8 %) when OIF were not included (Table 10). Based on literature, leaf-off ALS data should discriminate between coniferous and broadleaved tree species better than leaf-on ALS data. It appears that M-ALS does discriminate between the two groups, similar to leaf-off-UALS. Also, the volumes of pine and spruce were predicted noticeably better with M-ALS data than with leaf-off-UALS data. (Figure 3).

The MD% values for all the response variables using the different data combinations in the Liperi study area are presented in Table 11. Here, the results are interpreted as unsigned values (|MD%|). whereas in Table 11 the results are displayed as signed values. In general, the inclusion of OIF decreased the |MD%| values in both the LiDAR and IPC data. The |MD%| value was very high with the IPC data. Inclusion of OIF reduced the |MD%| values most in the case of broadleaved trees, although the respective reduction in |MD%| values of leaf-off-U-ALS was marginal with respect to broadleaved trees. With the IPC data, the |MD%| values of most volume predictions were noticeably reduced when OIF were used.

Table 10. Mean root mean square error (RMSE%) values obtained for pine, spruce, broadleaved and total volume in the test plots in the Liperi study area using the different methods.

	Mean RMSE% without optical image features	Mean RMSE% with optical image features
Leaf-on-UALS	62.8	33.3
Leaf-off-UALS	48.8	34.3
M-ALS	44.7	35.2
IPC	98.9	42.4

Table 11. Mean difference (MD%) of species-specific tree volume and total volume using leaf-off airborne Light Detection and Ranging (LiDAR), leaf-on airborne LiDAR, multispectral airborne LiDAR (M-ALS) and image point clouds (IPC) data with and without optical image features (OIF) in the validation field plots. Values in parenthesis indicates MD% values when OIF were included.

	Pine	Spruce	Broadleaved	Total
Leaf-on-UALS	3.6 (-6.3)	-2.1 (-2.5)	-18.8 (-4.8)	-2.9 (-4.4)
Leaf-off-UALS	-4.0 (-5.8)	-0.4 (-0.1)	-14.8 (-13.5)	-4.4 (-4.7)
M-ALS	1.5 (-3.5)	-2.6 (-2.3)	-12.5 (-7.3)	-2.8 (-3.6)
IPC	-8.0 (-3.1)	33.8 (12.3)	-28.4 (1.2)	6.5 (4.3)

5 DISCUSSION

This thesis continues the recurring discussion on how the selection of remote sensing data sources affects the performance of forest inventories by tree species. The contribution of this thesis to this discussion are primarily the advantages and the disadvantages of using only a single data source, as opposed to the combined use of multiple data sources. Commonly, optical image features, derived from aerial images, are used alongside ALS-based features to predict tree species-specific forest attributes. However, recent advances in both software and hardware have allowed for the collection of structural and optical information using a single sensor. The aim of this thesis was to compare the prediction errors of forest attributes when using image point clouds, made using stereo matching of aerial images, or multispectral ALS data, compared to the combined use of single wavelength leaf-on or leaf-off ALS data and optical image data. The results provide an insight on whether it is feasible to conduct remote sensing-based tree species-specific forest inventories using only data from a single airborne sensor. As the different data sources are evaluated based solely on their respective performances in predicting forest attributes, discussion regarding the implications for acquisition costs can be left for later studies.

In a forest inventory context, aerial images are undeniably a more abundant data source than LiDAR data, as aerial images are also commonly acquired periodically for purposes other than forestry, such as mapping and surveying (Stepper et al. 2017). LiDAR data, on the other hand, are generally collected from large forest areas for specific purposes, such as DTM generation, and are acquired less frequently. Thus, aerial images and their derivatives have notable potential in operational forestry applications as a stand-alone data source, as well as providing supporting data for LiDAR.

The results of this thesis corroborate that optical image features are beneficial in the prediction of tree species-specific forest attributes in a boreal forest environment in Finland. Inclusion of optical image features mainly improved species-specific predictions, specifically minority tree species. The prediction of total volume was less affected by the inclusion of optical image features. This is an expected result, as the structural information of LiDAR is assumed to correlate with the total forest attributes, while the reflectance of tree canopies is considered to contain information relevant for tree species discrimination. As observed in study **III**, the prediction error of the summed tree species-specific volume predictions was marginally reduced by the addition of optical image features, while the prediction errors associated with tree species volumes were noticeably reduced. This can be because similar sized trees generally result in similar volume predictions, regardless of tree species.

Stereo matching of aerial images is emerging as an alternative data source for forest inventories. With similar properties to LiDAR data, the data are easy to integrate into existing computation routines. However, the most notable distinctions between the two data sources are that the density of the canopy and the ground beneath the canopy are not well characterized by stereo matching data. These differences can cause fundamental problems when stereo matching data are used in the prediction of forest attributes. Currently, there is no available solution that would allow stereo matching to provide information from within the canopy. In addition, without external DTM the AGL heights are prone to errors in areas where the ground is obscured by a dense canopy (e.g. Graham et al. 2019). As observed in study **I**, the lack of accurate ALS-based DTM may increase the prediction errors of some forest attributes but the prediction errors of basal area and total growing stock volume were

similar both with and without ALS DTM, and the prediction error of stem number was only marginally increased. The availability of nationwide ALS data and ALS DTM is rapidly increasing in many countries. As topography rarely changes drastically over time, DTM can be used in other campaigns in the future without having to collect new ALS data for DTM purposes.

In accordance with the findings from a number of previous studies (e.g. Bohlin et al. 2012, Järnstedt et al. 2012, White et al. 2015), the ALS data in this thesis yielded lower prediction errors for forest attributes than stereo matching data. Also, the differences in prediction errors associated with total volume and tree species volumes between ALS and stereo matching data observed in studies **I** & **III** were similar to those reported in studies where stereo matching was compared to ALS in a boreal forest biome (e.g. Kangas et al. 2018). While the results might not be comparable between different geographical areas, the majority of current literature, including this thesis, agree that ALS data outperforms stereo matching data in the prediction of forest attributes. However, it should be noted that with respect to prediction errors, the differences between these two data sources is large between studies.

In this thesis, M-ALS data alone did not perform as well as U-ALS$_{(+OIF)}$ in the prediction of tree species-related attributes. The M-ALS data were outperformed by U-ALS$_{(+OIF)}$ data both in classifying dominant tree species and predicting the proportions of tree species in study **II**, and in predicting tree species volumes in study **III**. The difference in prediction errors between M-ALS and U-ALS$_{(+OIF)}$ were marginal in the classification of dominant tree species. The differences were, however, more pronounced in the prediction of tree species composition and in the prediction of tree species volumes. When classifying dominant tree species, the improvement in the classification accuracy when using only M-ALS or U-ALS$_{(+OIF)}$ compared to U-ALS were mainly attributable to the increased classification accuracy in the broadleaved plots. From this observation, a conclusion can be drawn that the intensity features of M-ALS data can provide information relevant to the classification between the two groups: conifer and broadleaved, similarly to optical image features. The prediction errors of both tree species composition and tree species volumes were reduced by using M-ALS compared to U-ALS. Therefore, the multispectral features of M-ALS data can, to a certain degree, distinguish between tree species, albeit not to the same extent as optical image features. These observations are supported by previous studies, which conclude that LiDAR intensity is, in addition to spectral reflectance, largely affected by the canopy conditions of the forest area (e.g. Korpela et al. 2010b). As the canopy conditions of broadleaved and coniferous tree species are particularly distinctive, LiDAR intensity should be well suited to distinguish between the two tree-classes, as observed in the case of the M-ALS intensity data in this thesis. Similar findings have been reported in literature. For example, Kim et al. (2009) concluded that LiDAR intensity can be used to distinguish broadleaved tree species from coniferous tree species.

Most of the previous studies where forest attributes have been predicted using M-ALS data have applied the ITD approach (Yu et al. 2017; Axelsson et al. 2018; Budei et al. 2018). Classifying field plots (with ABA) is different as field plots usually consist of a variety of tree species, whereas a delineated tree crown may consist of a single tree species. ABA aims to classify either dominant tree species or proportions of tree species, while the goal in ITD is to classify individual trees. Also, ITD approaches have disadvantages when tree-level predictions are aggregated to a larger area, due to tree detection and delineation errors.

The intensities of M-ALS are considered beneficial in the classification of tree species, both using ABA (Dalponte et al. 2018; Räty et al. 2019) and ITD (Yu et al. 2017; Axelsson et al. 2018; Budei et al. 2018). Although prediction errors or classification accuracies are not

directly comparable between ITD and ABA, we can examine whether similar features were important predictors. It should be noted that ITD features might benefit more from the increased point density of M-ALS than ABA (Gobakken & Naesset 2008). Therefore, the pivotal benefit of M-ALS in tree species-specific ABA should be in the novel features computed from the echoes of three LiDAR wavelengths. In this thesis, these features were calculated from the intensities of a combined set of echoes from two wavelengths (1064 nm and 1550 nm).

To the best of this author's knowledge, only two studies, in addition to this thesis, have applied ABA in the prediction of boreal tree species attributes using M-ALS. Räty et al. (2019) found that M-ALS features slightly decreased the prediction errors associated with logwood volumes compared to features calculated from U-ALS data. Dalponte et al. (2018) predicted the Shannon diversity index of tree species. In their experiment, using all three M-ALS channels performed better ($R^2 = 0.85$) than using only U-ALS data ($R^2 = 0.80$). They also reported that intensity features were important predictors of Shannon diversity index. It is difficult to compare the results of this thesis and the results of Dalponte et al. (2018), as predicting species richness is not directly relatable to predicting tree species composition. Similar to the results of this thesis, Dalponte et al. (2018) found that intensities from a combined set of echoes from different channels were beneficial. In this thesis, intensities of a combined set of echoes from two wavelengths were beneficial in tree species discrimination, although the intensity ratios of the different M-ALS features were not apparently important. One possible solution to further improve the classification accuracy of M-ALS, would be to filter the point cloud to only include points that have comparable observations to similar incidence angles from all other channels, although the 532 nm channel could not have sufficient observations remaining after the filtering process due to the smaller number of original observations.

In this thesis, the definition and requirement of a single sensor system is that both structure and optical image features can be acquired using a single instrument. Such a setup offers advantages, not specific to ABA, but also in inventories using the ITD approach. However, ITD may not benefit from optical image features as much as ABA because ITD can, to a certain extent, utilize the geometry of tree crowns (Li et al. 2013) or features of full-waveform LiDAR data (Yao et al. 2012) in tree species classification. Recognizing this, it is difficult to foresee how single sensor systems will be developed and utilized in future forest inventories. Nonetheless, the demand for a single sensor solution for forest inventories by tree species can be expected to increase as the acquisition of airborne data is progressively shifted to smaller unmanned platforms.

6 CONCLUSIONS

Based on the results of this thesis, both stereo matching of aerial images and M-ALS appear promising for tree species-specific forest inventories. Both data sources can be easily incorporated into existing forest inventory routines.

Stereo matching data, either with or without optical image features, do not perform as well as U-ALS or U-ALS$_{(+OIF)}$ data in predicting total volumes but do perform almost as well as U-ALS$_{(+OIF)}$ data in predicting tree species volumes. In contrast, M-ALS data perform more or less equally with U-ALS and U-ALS$_{(+OIF)}$ in predicting total volumes but are not comparable to U-ALS$_{(+OIF)}$ in predicting tree species volumes. Both stereo matching data and M-ALS data do provide lower prediction errors for tree species volumes than U-ALS data alone.

Despite the fact that stereo matching data are widely available, their use in forest inventories may be restricted to areas where ALS DTM is available. M-ALS does not have this restriction but, on the other hand, is a substantially more expensive data source than stereo matching data. This thesis has demonstrated the potential of M-ALS data for the prediction of species-specific stand attributes under the requirements of Finnish forestry.

REFERENCES

Alonzo M., Andersen H., Morton D.C., Cook B.D. (2018). Quantifying Boreal Forest Structure and Composition Using UAV Structure from Motion. Forests 9(3): 119. https://doi.org/10.3390/f9030119

Axelsson A., Lindberg E., Olsson H. (2018). Exploring Multispectral ALS Data for Tree Species Classification. Remote Sensing 10(2): 183. https://doi.org/10.3390/rs10020183

Axelsson P. (2000) DEM Generation from Laser Scanner Data Using Adaptive TIN Models. International Archives of the Photogrammetry, Remote Sensing and Spatial Information Sciences 33(B4/1): 110-117.

Andrews G.S. (1933). The use of aerial photographs In Forest surveying. Forest Surveys Division, BC Forest Service, Victoria, BC. https://doi.org/10.5558/tfc9033-4

Bohlin J., Wallerman J., Fransson J.E.S. (2012). Forest variable estimation using photogrammetric matching of digital aerial images in combination with a high-resolution DEM. Scandinavian Journal of Forest Research 27(7): 692–699. https://doi.org/10.1080/02827581.2012.686625

Bolles R. C., Baker H. H., Marimont D. H. (1987). Epipolar - plane image analysis: An approach to determining structure from motion. International Journal of Computer Vision 1: 755. https://doi.org/10.1007/BF00128525

Budei B.C., St-Onge B., Hopkinson C., Audet F. (2018). Identifying the genus or species of individual trees using a three-wavelength airborne lidar system Remote Sensing of Environment 204(1): 632-647. https://doi.org/10.1016/j.rse.2017.09.037

Cao L., Coops, N.C., Innes J.L., Dai J., Ruan H., She G. (2016). Tree species classification in subtropical forests using small-footprint full-waveform LiDAR data. International Journal of Applied Earth Observation and Geoinformation 49: 39–51. https://doi.org/10.1016/j.jag.2016.01.007

Chen T., Li W. (2017). Stereo matching algorithm based on adaptive weight and local entropy. 9th International Conference on Modelling, Identification and Control (ICMIC), Kunming Jul: 630–635. https://doi.org/10.1109/ICMIC.2017.8321532

Coren F., Sterzai P. (2006). Radiometric correction in laser scanning. International Journal of Remote Sensing 27(15): 3097–3104. https://doi.org/10.1080/01431160500217277

Dalponte M., Ene L. T., Gobakken T., Næsset E., Gianelle D. (2018). Predicting Selected Forest Stand Characteristics with Multispectral ALS Data. Remote Sensing 10(4): 586. https://doi.org/10.3390/rs10040586

Dash J.P., Pearse G.D., Watt M.S., Paul T. (2017). Combining Airborne Laser Scanning and Aerial Imagery Enhances Echo Classification for Invasive Conifer Detection. Remote Sensing 9: 156. https://doi.org/10.3390/rs9020156

Donoghue D. N. M., Watt P. J., Cox N. J., Wilson J. (2007). Remote Sensing of Species Mixturesin Conifer Plantations Using LiDAR Height and Intensity Data. Remote Sensing of Environment. 110(4): 509–522. https://doi.org/10.1016/j.rse.2007.02.032

Eerikäinen K. (2009). A Multivariate Linear Mixed-Effects Model for the Generalization of Sample Tree Heights and Crown Ratios in the Finnish National Forest Inventory. Forest Science 55(6): 480–493. https://doi.org/10.1093/forestscience/55.6.480

Gatziolis D., Andersen, H.-E. (2008). A guide to LIDAR data acquisition and processing for the forests of the Pacific Northwest. General Technical Report PNW-GTR-768. Portland, OR: U.S. Department of Agriculture, Forest Service, Pacific Northwest Research Station. 32 p. https://doi.org/10.2737/PNW-GTR-768

Giannetti F., Chirici G., Gobakken T., Næsset E., Travaglini D., Puliti S. (2018). A new approach with DTM-independent metrics for forest growing stock prediction using UAV photogrammetric data. Remote Sensing of Environment 213: 195-205. https://doi.org/10.1016/j.rse.2018.05.016

Gobakken T., Naesset E. (2008). Assessing effects of laser point density, ground sampling intensity, and field sample plot size on biophysical stand properties derived from airborne laser scanner data. Canadian Journal of Forest Research 38(5): 1095–1109. https://doi.org/10.1139/X07-219

Gobakken T., Bollandsås O.M., Næsset E. (2015). Comparing biophysical forest characteristics estimated from photogrammetric matching of aerial images and airborne laser scanning data. Scandinavian Journal of Forest Research 30(1): 73–86. https://doi.org/10.1080/02827581.2014.961954

Graham A., Coops N.C., Wilcox M., Plowright A. (2019). Evaluation of Ground Surface Models Derived from Unmanned Aerial Systems with Digital Aerial Photogrammetry in a Disturbed Conifer Forest. Remote Sensing 11(1): 84. https://doi.org/10.3390/rs11010084

Gupta R., Cho S. (2010). A correlation-based approach for real-time stereo matching. Advances in Visual Computing. Lecture Notes in Computer Science 6454(2): 129–138. https://doi.org/10.1007/978-3-642-17274-8_13

Haala N., (2011) Multiray photogrammetry and dense image matching. In Fritsch, D., editor, Photogrammetric Week, 11: 185–195.

Hastie T., Tibshirani R., Friedman J. H. (2009). The elements of statistical learning: Data mining, inference, and prediction. New York, USA: Springer ISBN 978-0-387-84858-7

Hill R.A., Wilson A.K., George M., Hinsley S.A., (2010). Mapping tree species in temperate deciduous woodland using time-series multi-spectral data. Applied Vegetation Science 13(1): 86–99. https://doi.org/10.1111/j.1654-109X.2009.01053.x

Hirschmüller H. (2008). Stereo Processing by Semi-Global Matching and Mutual Information. IEEE Transactions on Pattern Analysis and Machine Intelligence 30(2): 328–341. https://doi.org/10.1109/TPAMI.2007.1166

Hirschmüller H., Buder M., Ernst I. (2012). Memory efficient semi-global matching. ISPRS Annals of the Photogrammetry, Remote Sensing and Spatial Information Sciences 1(3): 371–376. https://doi.org/10.5194/isprsannals-I-3-371-2012

Holmgren J., Persson Å., Söderman U. (2008) Species identification of individual trees by combining high resolution LiDAR data with multi-spectral images. International Journal of Remote Sensing 29(5): 1537–1552. https://doi.org/10.1080/01431160701736471

Hyyppä J., Inkinen M. (1999). Detecting and estimating attributes for single trees using laser scanner. Photogrammetric Journal of Finland 16: 27–42, 1999.

Hyyppä J., Schardt M., Haggren H., Koch B., Lohr U., Scherrer H.U., Paananen R., Luukkonen H., Ziegler M., Hyyppä H., Pyysalo U., Friedländer H., Uuttera J., Wagner S., Inkinen M., Wimmer A., Kukko A., Ahokas E., Karjalainen M. (2001). HIGH-SCAN: the first European-wise attempt to derive single-tree information from laser scanner data. The Photogrammetric Journal of Finland 17(2): 58–68.

Jelalian A. (1992). Laser Radar Systems. Artech House. ISBN 978-0890065549

Jin M., Maruyama T. (2012). A fast and high quality stereo matching algorithm on FPGA. 22nd International Conference on Field Programmable Logic and Applications (FPL). Aug: 507–510. http://dx.doi.org/10.1109/FPL.2012.6339266

Järnstedt J., Pekkarinen A., Tuominen S., Ginzler C., Holopainen M., Viitala R. (2012). Forest variable estimation using a high-resolution digital surface model. ISPRS Journal of Photogrammetry and Remote Sensing, 74: 78–84. https://doi.org/10.1016/j.isprsjprs.2012.08.006.

Kangas A., Gobakken T., Puliti S., Hauglin M., Naesset E. (2018). Value of airborne laser scanning and digital aerial photogrammetry data in forest decision making. Silva Fennica 52(1): 9923. https://doi.org/10.14214/sf.9923

Kim S., McGaughey R. J., Andersen H.-E., Schreuder G. (2009). Tree species differentiation using intensity data derived from leaf-on and leaf-off airborne laser scanner data. Remote
Sensing of Environment 113(8): 1575–1586. https://doi.org/10.1016/j.rse.2009.03.017

Konecny G. (1985). The International Society for Photogrammetry and Remote Sensing - 75 Years Old, or 75 Years Young. Keynote Address. Photogrammetric Engineering and Remote Sensing 51(7): 919–933.

Korpela I., Tuomola T., Välimäki E. (2007). Mapping forest plots: an efficient method combining photogrammetry and field triangulation. Silva Fennica 41(3): 457–469. https://doi.org/10.14214/sf.283

Korpela I., Orka H. O., Hyyppä, J., Heikkinen V., Tokola T. (2010a). Range and AGC normalization in airborne discrete-return LiDAR intensity data for forest canopies. ISPRS Journal of Photogrammetry and Remote Sensing 65(4): 369–379. https://doi.org/10.1016/j.isprsjprs.2010.04.003

Korpela I., Ørka H.O., Maltamo M., Tokola T., Hyyppä J. (2010b). Tree species classification using airborne LiDAR – effects of stand and tree parameters, downsizing of training set, intensity normalization, and sensor type. Silva Fennica 44(2): 319–339. https://doi.org/10.14214/sf.156

Krabill W.B., Collins J.G., Link, L.E. Swift R.N., Butler M.L. (1984). Airborne laser topographic mapping results. Photogrammetric Engineering and Remote Sensing 50(6): 685–694.

Kukkonen M., Korhonen L., Maltamo M., Suvanto A., Packalen P., (2018). How much can airborne laser scanning based forest inventory by tree species benefit from auxiliary optical data? International Journal of Applied Earth Observation and Geoinformation 72: 91–98. https://doi.org/10.1016/j.jag.2018.06.017.

Laasasenaho J. (1982). Taper curve and volume functions for pine, spruce and birch. Communicationes Instituti Forestalis Fenniae 108. 74 p. ISBN 951-40-0589-9

Lefsky M.A., Cohen W.B., Parker, G.G., Harding D.J. (2002) Lidar remote sensing for ecosystem studies. Bioscience 52(1): 19–30. https://doi.org/10.1641/0006-3568(2002)052[0019:LRSFES]2.0.CO;2

Levick S. R., Hessenmöller D., Schulze E. D. (2016). Scaling wood volume estimates from inventory plots to landscapes with airborne LiDAR in temperate deciduous forest. Carbon balance and management 11(1): 1–14. https://doi.org/10.1186/s13021-016-0048-7

Li J., Baoxin Hu B., Noland T.L. (2013). Classification of tree species based on structural features derived from high density LiDAR data Agricultural and Forest Meteorology 171–172: 104–114. https://doi.org/10.1016/j.agrformet.2012.11.012

Lim J., Kim Y., Lee S. (2016) A census transform-based robust stereo matching under radiometric changes. Asia-Pacific Signal and Information Processing Association (APSIPA) Dec: 1–4. https://doi.org/10.1109/APSIPA.2016.7820841

Liu, Y., Monteiro S.T., Saber, E. (2015) An approach for combining airborne LiDAR and high-resolution aerial color imagery using Gaussian processes. Proc. SPIE 9643, Image and Signal Processing for Remote Sensing XXI, 96430Z (October 15, 2015); https://doi.org/10.1117/12.2194096

Maclean G.A. Krabill W.B. (1986). Gross-merchantable timber volume estimation using an airborne lidar system. Canadian Journal of Remote Sensing 12(1): 718. https://doi.org/10.1080/07038992.1986.10855092

Maltamo M., Eerikäinen K., Packalén P., Hyyppä J. (2006). Estimation of stem volume using laser scanning based canopy height metrics. Forestry 79: 217–229.

May N.C. (2008). A Rigorous Approach to Comprehensive Performance Analysis of State-of the-Art Airborne Mobile Mapping Systems, PhD dissertation, The Ohio State University.

Mayer N., Ilg E., Husser P., Fischer P., Cremers D., Doso-vitskiy A., Brox T. (2016). A large dataset to train convolutional networks for disparity, optical flow, and scene flow estimation. In: Conference on Computer Vision and Pattern Recognition, June 2016 https://doi.org/10.1109/CVPR.2016.438

Moeur M., Stage A. R. (1995). Most similar neighbor: An improved sampling inference procedure for natural resource planning. Forest Science 41(2): 337–359. https://doi.org/10.1093/forestscience/41.2.337

Næsset E. (1997). Estimating timber volume of forest stands using airborne laser scanner data. Remote Sensing of Environment 61(2): 246–253. https://doi.org/10.1016/S0034-4257(97)00041-2

Næsset E. (2002). Predicting forest stand characteristics with airborne scanning laser using a practical two-stage procedure and field data, Remote Sensing of Environment 80(1): 88–99 https://doi.org/10.1016/S0034-4257(01)00290-5.

Næsset, E. (2004). Practical large-scale forest stand inventory using small-footprint airborne scanning laser. Scandinavian Journal of Forest Research 19(2): 164–179. https://doi.org/10.1080/02827580310019257

Nelson R. (2013). How did we get here? An early history of forestry lidar. Canadian Journal of Remote Sensing 39: S6–S17. https://doi.org/10.5589/m13-011

Näslund M. (1937). Skogsförsöksanstaltens gallringsförsök i tallskog. Meddelanden från Statens Skogsförsöksanstalt, 29: 169.

Okutomi M., Kanade T. (1993). A multiple-baseline stereo. IEEE Transactions on Pattern Analysis and Machine Intelligence 15(4): 353–363. https://doi.org/10.1109/34.206955

Oliver C., Larson B. (1996). Forest Stand Dynamics. John Wiley and Sons.

Ørka H.O., Næsset E., Bollandsås O.M. (2007). Utilizing airborne laser intensity for tree species classification. International Archives of the Photogrammetry, Remote Sensing and Spatial Information Sciences 36: 300–304.

Ørka H.O., Dalponte M., Gobakken T., Næsse, E., Ene L.T. (2013). Characterizing forest species composition using multiple remote sensing data sources and inventory approaches. Scandinavian Journal of Forest Research 28(7): 677–688. https://doi.org/10.1080/02827581.2013.793386

Packalén P., Maltamo M. (2006). Predicting the plot volume by tree species using airborne laser scanning and aerial photographs. Forest Science 52(6): 611–622. https://doi.org/10.1093/forestscience/52.6.611

Packalén P., Maltamo M. (2007). The k-MSN method for the prediction of species-specific stand attributes using airborne laser scanning and aerial photographs. Remote Sensing of Environment 109(3): 328–341. https://doi.org/10.1016/j.rse.2007.01.005

Packalén P., Maltamo M. (2008). Estimation of species-specific diameter distributions using airborne laser scanning and aerial photographs. Canadian Journal of Forest Research 38(7): 1750–1760. https://doi.org/10.1139/X08-037

Packalén P., Suvanto A., Maltamo M., (2009). A Two Stage Method to Estimate Species-specific Growing Stock. Photogrammetric Engineering and Remote Sensing 75(12): 1451–1460. https://doi.org/10.14358/PERS.75.12.1451

Packalén P., Temesgen H., Maltamo M., (2012). Variable selection strategies for nearest neighbor imputation methods used in remote sensing based forest inventory. Canadian Journal of Remote Sensing 38(5): 557–569. https://doi.org/10.5589/m12-046.

Pepe M., Fregonese L., Scaioni M. (2018). Planning airborne photogrammetry and remote-sensing missions with modern platforms and sensors. European Journal of Remote Sensing 51(1): 412–436. https://doi.org/10.1080/22797254.2018.1444945

Persson M., Lindberg E., Reese H., (2018). Tree Species Classification with Multi-Temporal Sentinel-2 Data. Remote Sensing 10(11): 1794. https://doi.org/10.3390/rs10111794

Persson Å., Holmgren J., Söderman U. (2002). Detecting and measuring individual trees using an airborne laser scanner. Photogrammetric Engineering & Remote Sensing 68(9): 925–932. ISSN 0099-1112

Pitt D.G., Woods M., Penner M. (2014). A comparison of point clouds derived from stereo imagery and airborne laser scanning for the area-based estimation of forest inventory attributes in boreal Ontario. Canadian Journal of Remote Sensing 40(3): 214–232. https://doi.org/10.1080/07038992.2014.958420.

Puliti S., Gobakken T., Ørka H.O., Næsset E. (2017). Assessing 3D point clouds from aerial photographs for species-specific forest inventories. Scandinavian Journal of Forest Research 32(1): 68–79. https://doi.org/10.1080/02827581.2016.1186727

Rempel R.C., Parker A.K. (1964). An information note on an airborne laser terrain profile for micro-relief studies. In Proceedings of the 3rd Symposium on Remote Sensing of Environment (University of Michigan Institute of Science and Technology).

Räty J., Packalen P., Maltamo M., (2019). Nearest Neighbor Imputation of Logwood Volumes using Bi-temporal ALS, Multispectral ALS and Aerial Images. Scandinavian Journal of Forest Research. 34(6): 469–483. https://doi.org/10.1080/02827581.2019.1589567

Solodukhin V.I., Mazhugin I.N., Zhukov A.Y., Narkevich V.I., Popov Y.V., Kulyasov A.G., Marasin L.E., Sokolov S.A. (1979). Lazernaya aeros''emka profilei lesa (Laser aerial profiling of forest). Lesnoe Khozyaistvo 10: 4345. (in Russian)

Solodukhin V.I., Zhukov A.Y., Mazhugin, I.N. Narkevich V.I. (1976). Metody Izuchenija Vertikal'nyh Sechenij Drevostoev (Method of study of vertical sections of forest stands). Leningrad Scientific Research Institute of Forestry, Leningrad, USSR. 55 pp. (in Russian)

Standish M. (1945). The use of aerial photographs in forestry. Journal of Forestry 43(4): 252– 257. https://doi.org/10.1093/jof/43.4.252

St-Onge B., Vega C., Fournier R.A., Hu Y. (2008). Mapping canopy height using a combination of digital stereo-photogrammetry and LiDAR. International Journal of Remote Sensing 29(11): 3343–3364. https://doi.org/10.1080/01431160701469040

Seeley H. E. (1934). Aerial photography in forest surveys. Empire Forestry Journal 13(2): 244–247.

Seki A., Pollefeys M. (2017). Sgm-nets: Semi-global matching with neural networks. Sgm-nets: Semi-global matching with neural networks. In: Conference on Computer Vision and Pattern Recognition https://doi.org/10.1109/CVPR.2017.703

Stepper C., Straub C., Immitzer M., Pretzsch H. (2017). Using canopy heights from digital aerial photogrammetry to enable spatial transfer of forest attribute models: a case study in central Europe. Scandinavian Journal of Forest Research 32(8): 748–761. https://doi.org/10.1080/02827581.2 016.1261935

Straub C., Stepper C., Seitz R., Waser L.T. (2013). Potential of UltraCamX stereo images for estimating timber volume and basal area at the plot level in mixed European forests. Canadian Journal of Forest Research 43(8): 731–741. https://doi.org/10.1139/cjfr-2013-0125

Teledyne Optech (2019) http://info.teledyneoptech.com/acton/attachment/19958/f-02b6/1/-/-/-/-/Titan-Specsheet-150515-WEB.pdf [Cited 11 January 2019].

Tombari F., Mattoccia S., Di Stefano L., Addimanda E. (2008). Classification and evaluation of cost aggregation methods for stereo correspondence. IEEE Conference on Computer Vision and Pattern Recognition, Anchorage, AK June:. 1–8. https://doi.org/10.1109/CVPR.2008.4587677

Toth C. (2009). The State-of-the Art in Airborne Data Collection Systems – Focused on LiDAR and Optical Imagery. Photogrammetric Week '09 Dieter Fritsch (Ed.) Wichmann Verlag, Heidelberg

Tuominen S., Pitkänen T., Balázs A. and Kangas A. (2017). Improving Finnish Multi-Source National Forest Inventory by 3D aerial imaging. Silva Fennica 51(4): 7743. https://doi.org/10.14214/sf.7743

Törmä M. (2000). Estimation of tree species proportions of forest stands using laser scanning. International Archieves of Photogrammetry and Remote Sensing. ISPRS Congress Symposium 33: 1524–1531.

Ullah S., Dees M., Datta P., Adler P., Koch B. (2017). Comparing airborne laser scanning, and image-based point clouds by semi-global matching and enhanced automatic terrain extraction to estimate forest timber volume. Forests 8(6): 215. https://doi.org/10.3390/f8060215

Valbuena R., Mauro F., Arjonilla F.J., Manzanera J.A. (2011). Comparing airborne laser scanning-imagery fusion methods based on geometric accuracy in forested areas, Remote Sensing of Environment 115(8): 1942–1954. https://doi.org/10.1016/j.rse.2011.03.017

Vastaranta M., Wulder M.A., White J.C., Pekkarinen A., Tuominen S., Ginzler C., Kankare V., Holopainen M., Hyyppä J., Hyyppä H. (2013). Airborne laser scanning and digital stereo imagery measures of forest structure: Comparative results and implications to forest mapping and inventory update. Canadian Journal of Remote Sensing 39(5): 382–395. https://doi. org/10.5589/m13-046

Villikka M., Packalen P., Maltamo M. (2012). The suitability of leaf-off airborne laser scanning data in an area-based forest inventory of coniferous and deciduous trees. Silva Fennica 46(1): 99–110. https://doi.org/10.14214/sf.68

Wang Z., Boesch R., Ginzler C. (2007). Color and LIDAR Data Fusion: Application to automatic forest boundary delineation in aerial images. International Archives of Photogrammetry, Remote Sensing and Spatial Information Sciences 36: 4. https://doi.org/10.1109/IGARSS.2006.673

Wehr A., Lohr U. (1999) Airborne laser scanning—an introduction and overview. ISPRS Journal of Photogrammetry & Remote Sensing 54: 68–82. https://doi.org/10.1016/S0924-2716(99)00011-8

White J.C., Wulder M.A., Vastaranta M., Coops N.C., Pitt D., Woods M. (2013). The Utility of Image-Based Point Clouds for Forest Inventory: A Comparison with Airborne Laser Scanning. Forests 4(3): 518–536. https://doi.org/10.3390/f4030518

White J.C., Stepper C., Tompalski P., Coops N.C., Wulder M.A., (2015). Comparing ALS and Image-Based Point Cloud Metrics and Modelled Forest Inventory Attributes in a Complex Coastal Forest Environment. Forests 6(10): 3704-3732. https://doi.org/10.3390/f6103704

Wolter P., Mladenoff D.J., (1995). Improved Forest Classification in the Northern Lake States Using Multi-Temporal Landsat Imagery. Photogrammetric Engineering and Remote Sensing 61(9): 1129–1143.

Yao W., Krzystek P., Heurich M. (2012). Tree species classification and estimation of stem volume and DBH based on single tree extraction by exploiting airborne full-waveform LiDAR data. Remote Sensing of Environment 123: 368–380. https://doi.org/10.1016/j.rse.2012.03.027

Young M. (1986). Optics and Lasers—Series in Optical Sciences. Springer, Berlin, p. 145.

Yu X., Hyyppä J., Holopainen M. Vastaranta M. (2010). Comparison of Area-Based and Individual Tree-Based Methods for Predicting Plot-Level Forest Attributes. Remote Sensing 2(6): 1481–1495. https://doi.org/10.3390/rs2061481

Yu X., Hyyppä J., Karjalainen M., Nurminen K., Karila K., Vastaranta M., Kankare V., Kaartinen H., Holopainen M., Honkavaara E., Kukko A., Jaakkola A., Liang X., Wang Y., Hyyppä H., Katoh M. (2015). Comparison of laser and stereo optical, SAR and InSAR point clouds from air- and space-borne sources in the retrieval of forest inventory attributes. Remote Sensing 7(12): 15933–15954. https://doi.org/10.3390/rs71215809

Yu X., Hyyppä J., Litkey P., Kaartinen H., Vastaranta M., Holopainen M. (2017). Single-Sensor Solution to Tree Species Classification Using Multispectral Airborne Laser Scanning. Remote Sensing 9(2): 108. https://doi.org/10.3390/rs9020108

Zhang B., Miller S., DeVenecia K., Walker, S. (2006). Automatic terrain extraction using multiple image pair and back matching. Paper presented at ASPRS 2006 Annual Conference, Am. Soc. of Photogramm. and Remote Sens., Reno, Nevada, May 1–5.

Zhang B., Miller S., Walker S., Devenecia K. (2007). Next generation automatic terrain extraction using microsoft ultracam imagery. Paper presented at Proceedings of the ASPRS 2007 Annual Conference, Tampa, Florida, May 7–11.